Camera and projector calibration of an endoscopic fringe projection system

Steffen Matthias[1,*], Markus Kästner[1] and Eduard Reithmeier[1]

1 *Institute of Measurement and Automatic Control, Leibniz Universität Hannover,*

Nienburger Straße 17, 30167 Hannover, Germany

** Corresponding author: steffen.matthias@imr.uni-hannover.de*

Abstract:

In this paper, we present a method of an accurate camera and projector calibration for a newly developed endoscopic micro fringe projection system. The system consists of a laser illuminated digital micro-mirror device (DMD) for the projection of arbitrary structured light patterns, such as Gray code and cos²-phaseshift patterns. These patterns are focused into a 100'000 pixel image fiber and at the endpoint projected onto the specimen via gradient index lenses. A similar fiber assembly guides the perspective-distorted patterns back from the measurement object to a CCD-camera. The design for the areal measurement of filigree inner geometries generates new challenges for the camera and projector calibration, not only because of the reduced measurement area, but also because of the reduced resolution and artifacts of the image fibers. The camera is described by the standard pinhole camera model, while the projector is modeled using a black box. Calibration is performed by positioning a planar calibration rig with a linear stage. The linear stage is employed for partial automation of the calibration while the additional positioning data is combined with the information from the planar calibration rig to create a 3D data set for the calibration algorithm. This results in a considerably more robust identification of both the pinhole and black-box model. The capabilities of both models together with the developed calibration procedure are proven by the results of measurements of an inner gearing.

Keywords: 3D-measurement, endoscopy, fringe projection, laser projector, calibration

1. INTRODUCTION

Modern fabrication lines allow for a high automation of production processes. To minimize rejection costs, holistic inline inspection of parts and tools is desired. Optical measurement technologies are preferred for the task due to their ability to obtain contact free geometry data. An important requirement for inline inspection is a low measurement time in the range of one second or less. Depending on the task at hand, employed methods include fringe projection, confocal microscopy and white light interferometry. The technique used depends on the desired properties, e.g. the size of the measurement volume or whether geometry or surface data is to be gathered. Unfortunately, currently available systems for geometry inspection struggle to capture complex geometries with undercuts or internal structures. Shadows due to the geometry of the specimen or non-optimum measurement angles are challenges for the measuring device, which may lead to missing or noisy datasets.

The projects within the Transregional Collaborative Research Center 73 (SFB/TR73), supported by the German Research Foundation (DFG), develop a new cold sheet-bulk metal forming process with the objective of performing both deep drawing and bulk forming in a single fabrication step [1]. The goal of the scientific research is to reduce manufacturing times while maintaining low tolerances for the workpiece. One of the problems faced in the project is an inline inspection of the side elements of the forming tool, as shown in Fig. 1.

To allow for an inline inspection of the running process, a new kind of endoscopic fringe projection system has been developed. The new device features a compact sensor head, which is coupled to a base station using flexible image fibers. The benefit of this design in comparison to commercially available fringe projection systems is the ability to position the sensor head more freely towards the specimen. Different sensor head designs can be created to adapt to the requested task. A laser light source is used in the projector unit with the advantage of high light intensities. Measurement times using a sequence of 11 standard Gray-code and phase-shift patterns are currently in the range of 3 seconds.

Especially the image fibers and micro-optics employed in the sensor head pose a challenge for the algorithms for image processing, calibration and analysis. The low resolution of the image fibers and the reduced image contrast result in noisy calibration data, while the custom-built gradient-index optics exhibit distortions uncommon for conventional lenses. To achieve high quality measurements, the system model and the parameter identification algorithm need to be adapted to the system.

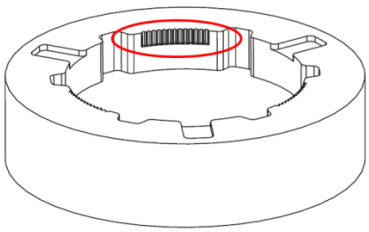

Fig. 1: TR73 Sheet bulk-metal forming demonstration tool with inner gearings [2].

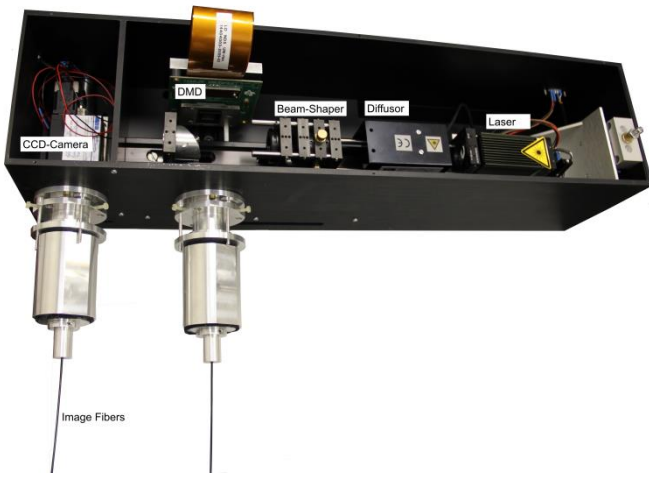

Fig. 2: Base station of the endoscopic fringe projection system.

2. DESCRIPTION OF THE OPTICAL SYSTEM

2.1 System Description

Figure 2 shows the base station unit of the newly developed endoscopic fringe projection system. A green frequency doubled Nd:YAG laser is used in the projector as the laser light can be efficiently coupled into the image fiber with high intensities. The complete assembly of the projector including the 100 mW laser is housed in a laser-safe casing.

To avoid speckle interference patterns, which appear when a coherent light source is projected onto a rough surface, a rotating diffusor is used. The rotating diffusor leads to temporal different speckle patterns, which even out over the exposure time when being captured by a camera. Following the diffusor, a beam shaper is placed in the optical path to generate a flat-top beam profile. The beam shaper consists of two micro-lens arrays and leads to a more homogenous illumination of the projector. A digital micro-mirror device (DMD) by Texas instruments is used to generate the fringe patterns. The DMD features a matrix of 1024 by 768 mirrors, which can be controlled independently

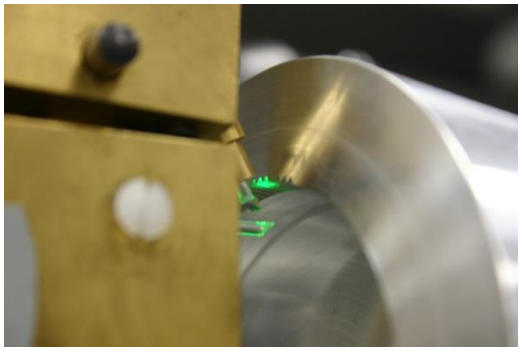

Fig. 3: Pattern projection on the SBMF-tool with GRIN optics.

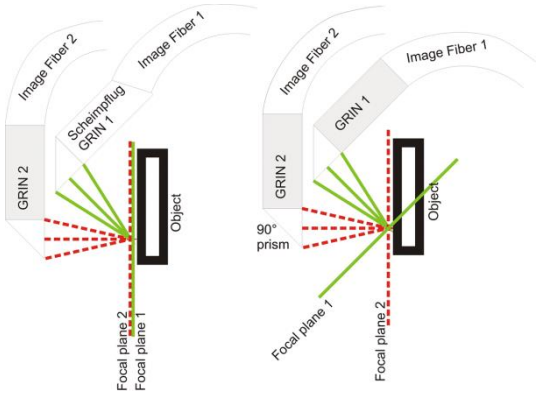

Fig. 4: Endoscopic fringe projection using Scheimpflug GRIN (left) and Standard GRIN optics (right) [4].

to create arbitrary patterns. The generated pattern is coupled into the image fiber and then projected onto the specimen via a gradient-index (GRIN) micro lens.

The detector side also uses a GRIN lens to capture the projected pattern into the second image fiber, which is connected to a CCD-camera. Both projector and detector fibers and GRIN lenses are located in the sensor head, which can see seen in Fig. 3.

2.2 Scheimpflug Gradient-Index Optics

To achieve good imaging quality in the measuring volume, fringe projection systems are often designed by the Scheimpflug principle [3]. Principal planes of projector and detector are aligned to each other. Figure 4 shows the adaption of the Scheimpflug principle for the endoscopic fringe projection system. Classical lenses are tilted to accomplish the tilted focal plane. For gradient-index lenses this is not feasible, as the flat lens surface is directly attached to the image fiber surface for efficient coupling.

To be able to align the focal planes better than using standard GRIN lenses, Ohrt developed a GRIN lens with modified geometry [4]. The lens is modified by grinding and polishing a tilted optical plane to the lens geometry to approximate the desired tilted image plane. As the geometry is an approximation to the ideal image surface, the image appears slightly distorted.

3. CALIBRATION APPROACH

3.1 System Models

The most common model to describe cameras and projectors is the pinhole model, which uses a projection matrix K, as seen in Eq. 1, to describe the projection from the camera centric 3D coordinate system to the 2D sensor coordinate system [5]. The principal point is modeled with the parameters c_x and c_y, while f_x and f_y describe pixel size and focal length.

$$K = \begin{bmatrix} f_x & 0 & c_x \\ 0 & f_y & c_y \\ 0 & 0 & 1 \end{bmatrix} \quad (1)$$

The transformation from an arbitrary coordinate system to the camera coordinate system can be described in homogenous coordinates by a transformation matrix T, where R is a 3x3 rotation matrix and t a 3x1 translation vector.

$$T = \begin{bmatrix} R & t \\ 0 & 1 \end{bmatrix} \quad (2)$$

The projection x of a 3D point X in an arbitrarily located coordinate system can be calculated in homogenous coordinates by Eq. 3.

$$x = KTX \quad (3)$$

Radial and tangential distortions can be compensated in the sensor coordinate system [6]. To fully describe a fringe projection system using this model, two projection matrices and a transformation matrix are needed. The projection matrices with optional distortion parameters describe the optical parameters of camera and projector according to the model, while the transformation matrix is used to define the rotation and translation from the projector coordinate system to the camera coordinate system or vice versa.

Extensions of the pinhole model to describe Scheimpflug optics exist [7]. One or more parameters are used to define a rotation of the tilted image plane towards the pinhole image plane.

An alternative to the pinhole model are black-box models, which use an appropriate mathematical function to describe the relation of phase to 3D-coordinate for each camera pixel, as shown in Eq. 2. Parameters u and v are the coordinates of a pixel in the sensor coordinate system, φ the phase value and p is the 3D point. Common for the task are polynomials.

$$p = f(\varphi, u, v) \quad (4)$$

Vargas describes a combination of the pinhole model and the black-box model for a fringe projection system [8]. The camera is modelled by the pinhole model, while the depth information and thus the projector optics are described by a black box similar to Eq. 4. Camera parameters are calibrated with the use of a planar calibration rig according to the approach by Zhang [9]. The captured phase-maps and the corresponding transformation matrices for each plane position are then used to calibrate the projector.

The standard pinhole model with additional Scheimpflug angle parameterization is not able to describe the modified GRIN optics very well. The radial and tangential distortion models do not match the inhomogeneous distortion induced by the image plane approximation described in Section 2.2. Thus, a black box model was chosen to calibrate the projector. Since a standard GRIN lens is used for the camera, the pinhole model will be used to calibrate the camera. The number of parameters to be identified using this approach is much lower compared to a black box model for both camera and projector.

3.2 Calibration Setup and Process

The calibration setup includes a plane dot grid standard from Edmund Optics and an Aerotech ATS100 linear stage. The standard is positioned on the linear stage so that the movement is perpendicular to the 2 axes defined by the pattern. The position of the stage can be controlled by the calibration software and with an accuracy of 2 µm.

To capture the information necessary for both camera and projector calibration, the sensor head is positioned in front of the calibration standard. It is not necessary to position the sensor head perpendicular to the standard, as the position and pose of this initial plane position will be calculated later during the calibration process. To capture the input for the calibration algorithm, the linear axis moves through the desired measurement volume with adequately low steps. Typical setup for the endoscopic system is a movement over a 3 mm distance in 0.1 mm steps.

The positioning information from the linear stage can be interpreted as the z-coordinate of the object points, effectively creating a 3D-calibration object. The correspondences from the detected marker positions in the sensor coordinate systems and the 3D object points are used in the calibration algorithm.

The camera calibration algorithm calculates the camera matrix, the distortion coefficients and the transformation matrix by minimizing the squared reprojection error [5]. An example of the camera calibration is shown in Fig. 5. It should be noted that although the points appear to be different planes, they are all located in the same coordinate system, forming a 3D-calibration object. Not all captured planes and markers are currently used for the camera calibration, due to the low S/N ratio in the camera image when detecting the markers on the calibration standard. However, the additional captured calibration planes are later employed in the projector calibration.

To generate the input for the black box calibration algorithm, first the initial position of the calibration plane needs to be known in the camera coordinate system. This information can be gathered from the transformation matrix, which describes the position and pose of the sensor head towards the initial plane position. The third column of the rotation matrix R in Eq. 2 is the normal vector n of the

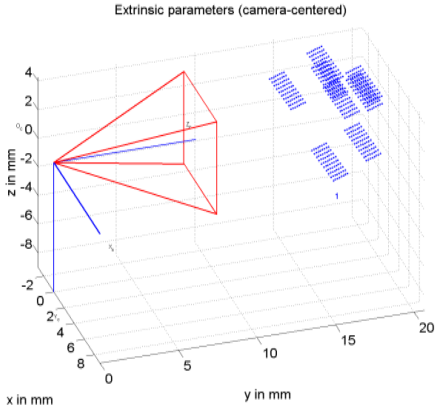

Fig. 5: Object points used for camera calibration.

planes at all positions, while the translation vector t is the position vector of the calibration plane at the first position before moving the axis. All other plane position vectors can be calculated by offsetting t with the axis position multiplied with the normal vector n. Now the necessary z-coordinates for each pixel at each plane position can be calculated by intersecting the ray r for each camera pixel (u,v), obtained by Eq. 5, with the plane equations of all captured positions.

$$r = K^{-1} \cdot s \cdot \begin{bmatrix} u \\ v \\ 1 \end{bmatrix} \tag{5}$$

The black box calibration algorithm uses 6th order polynomials to calculate the depth-to-phase relation for each pixel.

4. RESULTS

The quality of the calibration is improved significantly by employing the linear stage. Both camera and projector calibration benefit from the additional information and the thus lower number of extrinsic parameters to identify. Another aspect is the ability to capture a high number of calibration points, as the calibration object is moved automatically by the linear axis.

To evaluate the quality of the calibration, a plane standard was measured in an arbitrary position. The deviations from the best-fit plane are plotted as a measure of calibration quality. Fig. 6 shows the plane deviations after calibrating the system without using the linear axis. In comparison, the plane was measured in the same position after calibration with the linear axis in Fig. 7. It can be seen that the distribution in Fig. 6 is asymmetric and with a much higher standard deviation than in Fig. 7. It should also be noted, that the number of points in Fig. 6 is much lower, because a high number of sensor points were not calibrated correctly when calibrating without the linear axis. The standard deviation of the plane-fit error is about 9 µm when calibrating with the linear axis.

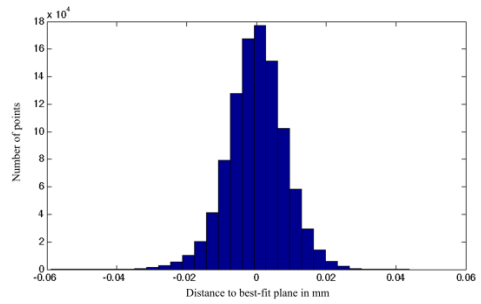

Fig. 6: Plane-fit deviations after calibration using the linear stage.

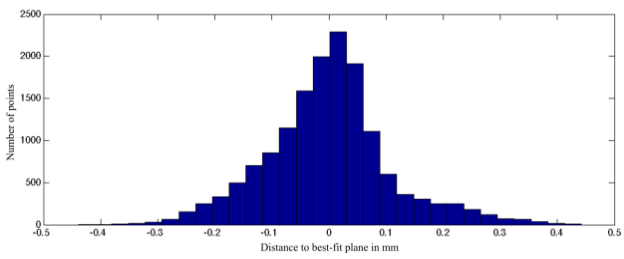

Fig. 7: Plane-fit deviations after calibration without the linear stage.

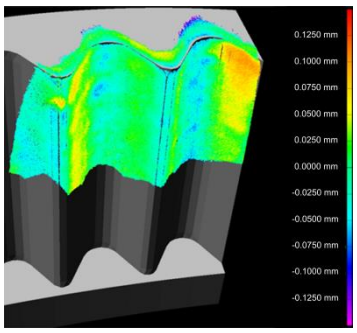

Fig. 8: Measurement of an inner gearing.

Fig. 8 shows a measurement of the inner gearing seen in Fig. 1. The standard deviation of the distance to the CAD-model is about 35 µm.

5. CONCLUSION AND OUTLOOK

A calibration approach was developed for the endoscopic fringe projection. It was shown that the calibration results were improved significantly, after a linear axis was added to the calibration setup and accounted for in the calibration algorithm.

To improve results further, the marker detection algorithm will be enhanced to capture more markers for the camera calibration algorithm. Another aspect is the filtering of the phase-map data in regard to the artifacts originated from the image fibers.

ACKNOWLEDGEMENTS

The authors would like to thank the German Research Foundation (DFG) for funding the project B6 "Endoscopic geometry inspection" within the Collaborative Research Center (CRC) / TR 73.

REFERENCES

[1] M. Merklein, J. M. Allwood, B. Behrens, A. Brosius, H. Hagenah, K. Kuzman, K. Mori, E. Tekkaya and A. Weckenmann, "Bulk forming of sheet metal", *CIRP Annals-Manufacturing Technology*, vol.61(2), pp. 725-745.

[2] C. Ohrt, W. Hartmann, J. Weickmann, M. Kästner, A. Weckenmann, T. Hausotte and E. Reithmeier, "Holistic Measurement in the Sheet-Bulk Metal Forming Process with Fringe Projection", *Key Engineering Materials*, vol.504, pp. 1005-1010.

[3] J. Carpentier, "Improvements in Enlarging or like Cameras" *British patent N°1139*, 1901.

[4] C. Ohrt, "Development of a Measuring Endoscope for the In-Line Quality Control of Filigree Form Elements in Forming Production Lines", PZH-Verlag, ISBN: 978-3-944586-41-0.

[5] R. Hartley and A. Zisserman, "Multiple View Geometry in Computer Vision", Cambridge University Press, ISBN: 0521540518.

[6] C. Brown, "Close-range camera calibration", PHOTOGRAMMETRIC ENGINEERING, vol.37(8), pp. 855-866.

[7] A. Legarda, A. Izaguirre, N. Arana, and A. Iturrospe, "A new method for Scheimpflug camera calibration", *Electronics, Control, Measurement and Signals (ECMS), 2011 10th International Workshop on*, pp. 1-5.

[8] J. Vargas, M.J. Terrón-López and J.A. Quiroga, "Flexible calibration procedure for fringe projection profilometry", *Optical Engineering*, vol.46(2), p. 023601.

[9] Z. Zhang, "A flexible new technique for camera calibration", *IEEE Transactions on Pattern Analysis and Machine Intelligence*, vol.22(11), pp. 1330-1334.